electronics

MDPI

Article

Control and Validation of a Reinforced Power Conversion System for Upcoming Bioelectrochemical Power to Gas Stations

Mahdi Shahparasti [1,*], Amirhossein Rajaei [2], Andres Tarraso [3], Jose David Vidal Leon Romay [3] and Alvaro Luna [3,*]

[1] School of Technology and Innovations, University of Vaasa, 65200 Vaasa, Finland
[2] Department of Electrical and Electronics Engineering, Shiraz University of Technology, Shiraz 71557-13876, Iran; a.rajaei@sutech.ac.ir
[3] Department of Electrical Engineering, Technical University of Catalonia, 08222 Barcelona, Spain; andres.tarraso@upc.edu (A.T.); davidromay90@gmail.com (J.D.V.L.R.)
* Correspondence: mahdi.shahparasti@uwasa.fi (M.S.); luna@ee.upc.edu (A.L.)

Abstract: This paper presents a proposal for potential bioelectrochemical power to gas stations. It consists of a two-level voltage source converter interfacing the electrical grid on the AC side and an electromethanogenesis based bioelectrochemical system (EMG-BES) working as a stacked module on the DC side. The proposed system converts CO_2 and electrical energy into methane, using wastewater as the additional chemical energy input. This energy storage system can contribute to dampening the variability of renewables in the electrical network, provide even flexibility and grid services by controlling the active and reactive power exchanged and is an interesting alternative technology in the market of energy storage for big energy applications. The big challenge for controlling this system lays in the fact that the DC bus voltage of the converter has to be changed in order to regulate the exchanged active power with the grid. This paper presents a cascade approach to control such a system by means of combining external control loops with fast inner loops. The outer power loop, with a proportional-integral (PI) controller with special limitation values and anti-windup capability, is used to generate DC bus voltage reference. An intermediate loop is used for DC bus voltage regulation and current reference generation. A new proportional resonant controller is used to track the current reference. The proposed scheme has been validated through real-time simulation in OPAL OP4510.

Keywords: biomethane; microbial electrochemical technologies; microgrid; proportional resonant controller; power to gas station

Citation: Shahparasti, M.; Rajaei, A.; Tarraso, A.; Vidal Leon Romay, J.D.; Luna, A. Control and Validation of a Reinforced Power Conversion System for Upcoming Bioelectrochemical Power to Gas Stations. *Electronics* **2021**, *10*, 1470. https://doi.org/10.3390/electronics10121470

Academic Editor: Gabriel Garcerá

Received: 24 May 2021
Accepted: 17 June 2021
Published: 18 June 2021

1. Introduction

The electricity production from renewable-based Distributed Generation (DG) technologies has rapidly increased due to the growth of electrical energy consumption and environmental concerns [1,2]. The integration of microgrids is a pathway to facilitating a flexible integration of DG, loads and energy storage systems [3,4]. In the microgrid, the loads and renewable-based energy resources have random and unpredictable behavior. Therefore, using energy storage systems and programmable generators is necessary to control the voltage, frequency and power exchanged with the upstream network [5,6]. The energy capacity constraint is the most significant limitation in common energy storage systems, such as batteries, leading to the development of new electrical energy storage solutions [7,8].

The production of CH_4 from CO_2 using renewable energy surplus, known as Power to Gas (P2G), represents a potential high-capacity energy storage technology [9–12]. The P2G process links the power grid with the natural gas grid by converting CO_2 and electrical energy into a grid-compatible, synthetic natural gas (mostly CH_4), increasing the overall resilience of the energy system and decreasing its price. The position and perspectives

of P2G plants for managing high contributions of renewable energies has been discussed previously [13].

H_2 production through water electrolysis represents the state-of-the-art for P2G technology; however, the gas distribution grid is not prepared for H_2, contrary to methane, which limits the energy storage capacity. Alternatively, the chemical and biological production of methane is implemented in several pilot plants, spread around Europe [14,15]. However, both methanation options present drawbacks, e.g., requirement of an expensive catalyst, high operating temperature and pressure and limited efficiency [14].

Bioelectrochemical systems performing electromethanogenesis (EMG-BES) were first proposed in 2009 as an alternative way to drive the reduction of CO_2 (dissolved into an aqueous medium) into CH_4 [16]. This represented a milestone for the development of likely processes, producing different added-value chemicals and fuels from CO_2 and renewable energy surplus [17]. The process is performed under mild operational conditions (20–35 °C and atmospheric pressure) and is driven by electroactive microorganisms, without the need of an expensive catalyst, meaning higher energy efficiency and potentially lower construction and operational costs compared to chemical methanation [18]. Thus, P2G based on EMG-BES represents an innovative and flexible energy storage technology for renewable energy surplus (RES) management. It offers a suitable solution for seasonal energy storage of RES, and it enables the convergence of an electrical grid with an existing natural gas grid into one hybrid energy system [19]. Besides, this technology can also help to reduce CO_2 emissions from industries, decarbonizing the electricity sector [20].

In this paper, bioelectrochemical power to gas stations based on an EMG-BES stack is discussed, based on preliminary data collected from a laboratory prototype [21]. The technology has the ability to receive active power and exchange reactive power with the grid (Figure 1). For achieving this goal, the proposed topology for the power converter, located upstream of the bioelectrochemical plant, is a two-level voltage source converter (2L-VSC) because: (1) the EMG-BES stack has to be fed by regulated DC voltage and (2) 2L-VSC can draw the sinusoidal current from the grid. Using 2L-VSC provides high power quality performance and grid support capability in contrast to other solutions such as diode rectifier and DC/DC converter in [22]. The conventional control schemes of grid-connected 2L-VSCs cannot be used directly for this system because they are only designed to control variables such as PQ (active/reactive powers), PV (active power/AC terminal voltage), $V_{dc}Q$ (DC link voltage/reactive power) and $V_{dc}V$ (DC link voltage/AC terminal voltage) [3]. However, V_{dc}, P and Q need to be controlled at the same time for this application. Recently, Reference [23] suggested a two-loop control scheme for BES applications that included an outer power loop and an inner current loop; however, this approach is not applicable because the DC link voltage must be controlled with 2L-VSC. Therefore, this paper proposes a control scheme that consists of three loops: an outer power loop, a middle DC link voltage loop and finally an inner current loop, which are implemented in the stationary reference frame. The contribution of the control scheme consists of three parts: (1) BES works a controlled PQ load with this method, (2) a new Proportional-Resonant (P + R) controller with harmonic compensation capability and anti-windup capability is to be used as the current controller and (3) a new DC-link voltage reference modifier, which defines the appropriate reference to keep the system stable. It is worth mentioning that the basic idea of this paper was already published by authors as a conference paper in [24].

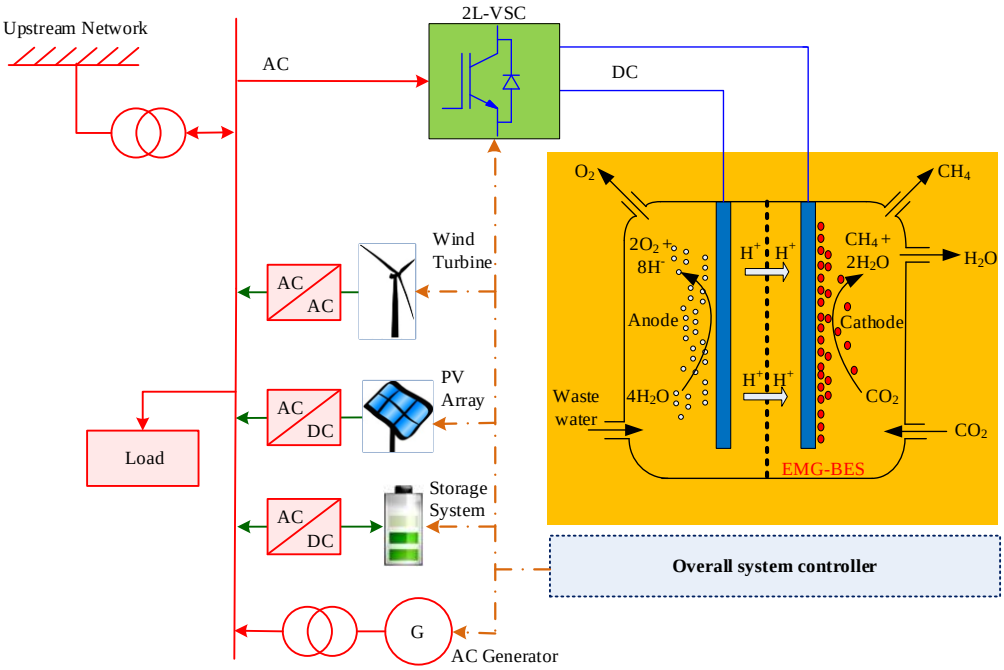

Figure 1. Schematic of a microgrid with bioelectrochemical power to gas station.

This paper is organized as follows. In Section 2, the EMG-BES based energy storage system is briefly introduced, and a medium-scale laboratory prototype is presented. In Section 3, the description of the proposed topology scheme for the electrical converter and its control system are presented. In Section 4, the simulation results that allowed us to analyze the performance of the proposed controller are presented. Finally, the conclusions arising from this work are presented in Section 5.

2. EMG-BES Stack

The standard BES reactor comprises an anode and a cathode, sometimes separated by an ionic exchange membrane [25]. In the case of the developed EMG-BES technology, the reactor is membrane-less, and an electrical input drives the set of anode and cathode reactions, which would be otherwise thermodynamically unfavorable. At the cathode, electro-autotrophic microorganisms utilize CO_2 as a carbon source and electricity as the source of reduction equivalents to produce CH_4 [26]. On the other hand, at the anode the organic matter contained in wastewater is oxidized by electroactive bacteria (EAB), transferring the required electrons to the cathode.

In [9], a medium-scale EMG-BES prototype was built by connecting 45 cells (i.e., each pair of electrodes) in parallel, grouped by 3 into 15 single-chamber, membrane-less reactor modules. The voltage stack was increased from 0.7 to 18 V to guarantee a voltage drop near 1–1.2 V for each series-connected module. The voltage drop of each EMG-BES cell needed to be balanced to allow the proper operation of the anode and cathode and to convert the electrical current into methane. A passive voltage balancing system was adopted [18].

The electrical stabilization time of the EMG-BES prototype, due to voltage variation from the open-circuit voltage (OCV) to operational voltage, was in the minute scale time. The peak of current observed when the voltage was applied was due to the self-capacitance of the bioelectrodes [27]. This capacitance was produced by the electrons accumulated at the anode due to the spontaneous oxidation of organic matter by EABs and the high surface area of carbon material used as the electrode.

In terms of electrical current conversion to methane, this was slower than the shown electrical dynamics, resulting in difficult-to-quantify electrical-driven CH_4 production [23]. This behavior (among other factors) caused the EMG-BES reactor to continue producing methane also when no energy input was applied.

Figure 2 shows experimental results of current vs. voltage for 15 parallel EMG-BES modules, wherein: (1) the level of current can be controlled by the input voltage; (2) the input voltage must be higher than 0.45 V and less than 1 V for linear operation of EMG-BES; moreover, a reverse current will flow into the DC source at low input voltages, and the EMG-BES saturates at voltages higher than 1 V, where the current remains constant and (3) all parallel modules behave similarly and tend to follow the same pattern. Therefore, the electrical characteristic of an EMG-BES pack, with several modules in series and parallel, can be interpreted from a module behavior since they operate together. In this paper, several modules are considered in parallel and series to make a 10 kW EMG-BES stack.

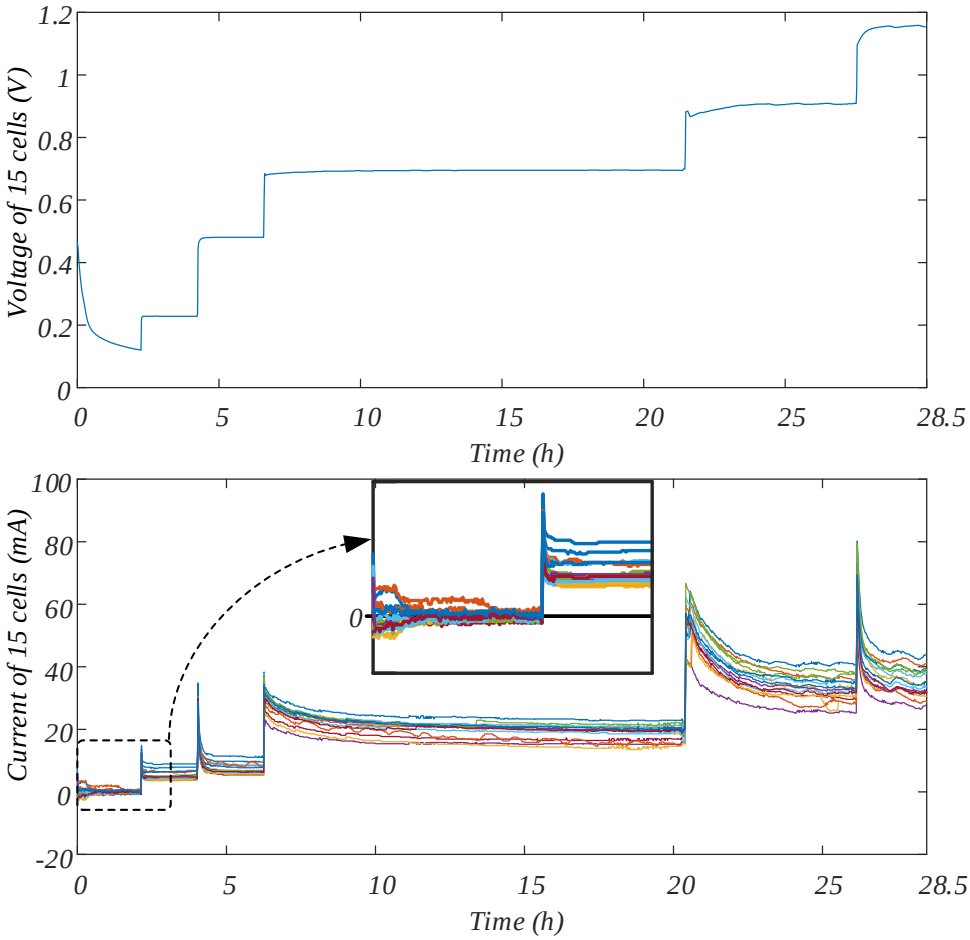

Figure 2. Current vs. voltage for 15 parallel EMG-BES cells.

The considered model for the EMG-BES cell is shown in Figure 3 [10,28]. The model parameters in Table 1 are chosen based on the method mentioned by [10] and data of experimental tests in the nominal state. In a stack with n_s series cell in each branch and n_p parallel branches, the following parameters can be used in the model:

$$\begin{aligned} E_{0,stack} &= n_s \times E_0, \\ C_{0,stack} &= \frac{n_p}{n_s} \times C_0, \\ R_{0,stack} &= \frac{n_s}{n_p} \times R_0, \\ R_{1,stack} &= \frac{n_s}{n_p} \times R_1. \end{aligned} \tag{1}$$

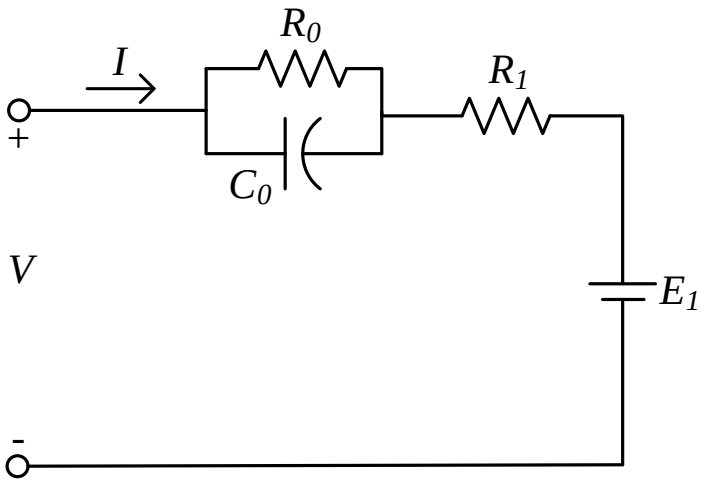

Figure 3. A dynamic model for EMG-BES stack.

Table 1. EMG-BES cell model parameters.

Parameter	Value
R_0 (Ω)	2.576
C_0 (F)	316.8
R_1 (Ω)	0.3193
E_1 (V)	0.115

3. Proposed Topology and Associated Control Scheme

According to Section 2, the EMG-BES stack must be fed by variable and regulated DC voltage to control the EMG-BES current. The applied voltage must be higher than the specific value (0.45 V for a cell with 0.7 V nominal voltage). Therefore, an AC/DC converter is required as an interface to connect the EMG-BES to the electrical grid. This paper proposes a 2L-VSC with an LCL filter for this purpose (Figure 4). The hardware design of 2L-VSC is explained in [29,30] and is out of the scope of this paper. This paper aims to develop a control scheme for this system to feed an EMG-BES with a regulated voltage. With this control method, the EMG-BES works as an active load that can absorb a controlled active power from the grid and is able to exchange reactive power with the grid. The converted energy inside the EMG-BES adds a new degree of freedom which can be exploited to provide ancillary services such as energy management, flexibility, frequency regulation, voltage profile improvement and power oscillation damping.

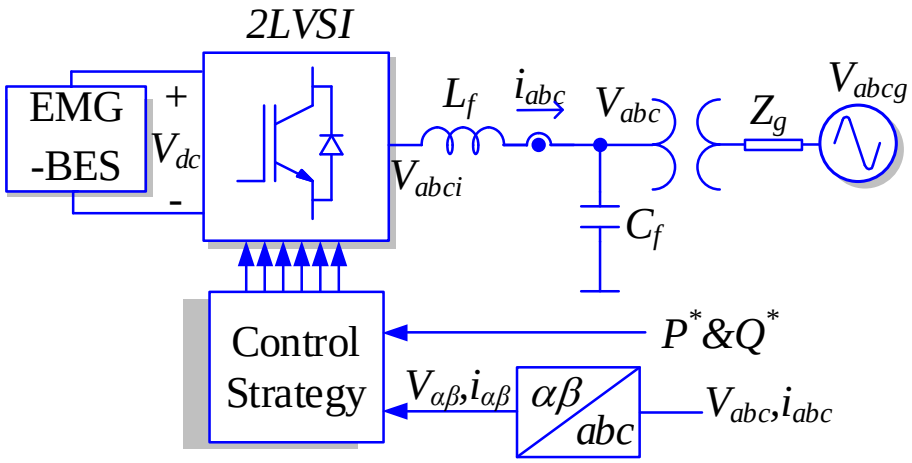

Figure 4. Overall schematic of the proposed bioelectrochemical power to gas station.

In this study, the overall system controller is supposed to send the power reference (P^* and Q^* in Figure 4) to the EMG-BES power plant. This power reference can be determined by distribution system operators (DSOs) to manage the grid by ancillary services. The latter, counting on a 2L-VSC converter as an interface with the grid, converts the power reference to a DC link voltage reference, then it is tracked by the voltage and current controller.

For the linear operation of 2L-VSC, the relationship between the DC side and AC side voltage can be expressed as in Equation (2) (see also Figure 5):

$$V_{dc} = \frac{2V_i}{m}, \tag{2}$$

where V_i, V_{dc} and m are the maximum phase voltages of the 2L-VSC, DC bus voltage and 2L-VSC modulation index, respectively. The maximum value of m for linear operation of the 2L-VSC depends on the switching method and can be a value between 1 and 1.154 [31]. In terms of controllability, 2L-VSC becomes uncontrollable for m higher than 1.1547; therefore, the DC bus voltage cannot reduce less than a specific value. This limitation must be considered in a loop scheme design.

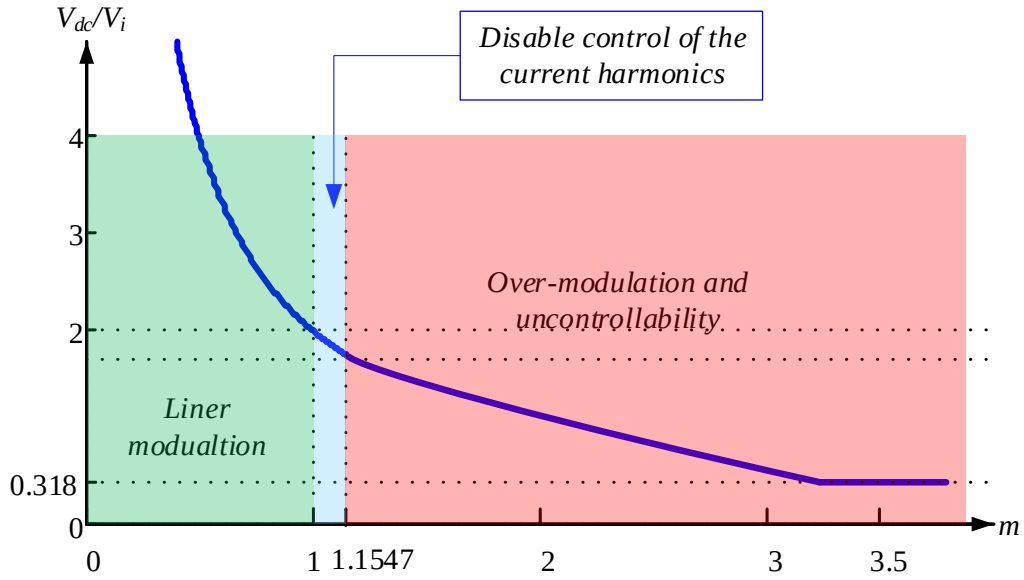

Figure 5. 2L-VSC gain (V_{dc}/V_i) vs. modulation index (m) in the rectification mode.

The proposed control scheme consists of three main parts: (1) The outer power loop for DC link voltage reference generation, (2) the middle DC link voltage loop and (3) the inner current loop with a new PR controller with harmonic compensation and anti-windup capabilities.

In the outer loop, according to Figure 6, the active power reference (P^*) is compared with the active output power of the 2L-VSC (P), generating an error value. Then, this error is the input of a PI controller, which determines at the output the initial DC link voltage reference $V_{dc\,ref}$. In the present application, the grid voltage is fixed, hence the 2L-VSC works in the linear region, the DC link voltage should be higher than the specific value (V_{dcmin}). The DC link voltage reference modifier is proposed to keep the 2L-VSC converter under control and also to avoid instabilities in the system. The output of the DC link voltage reference modifier (V_{dc}^*) is used as a reference value for the middle DC link voltage loop. The reference of current in the stationary reference frame can be found based on the output of the DC link voltage controller, reactive power reference and the positive sequence of PCC voltage. The current reference is tracked by the proposed proportional resonant controller with anti-windup and harmonic compensation capabilities.

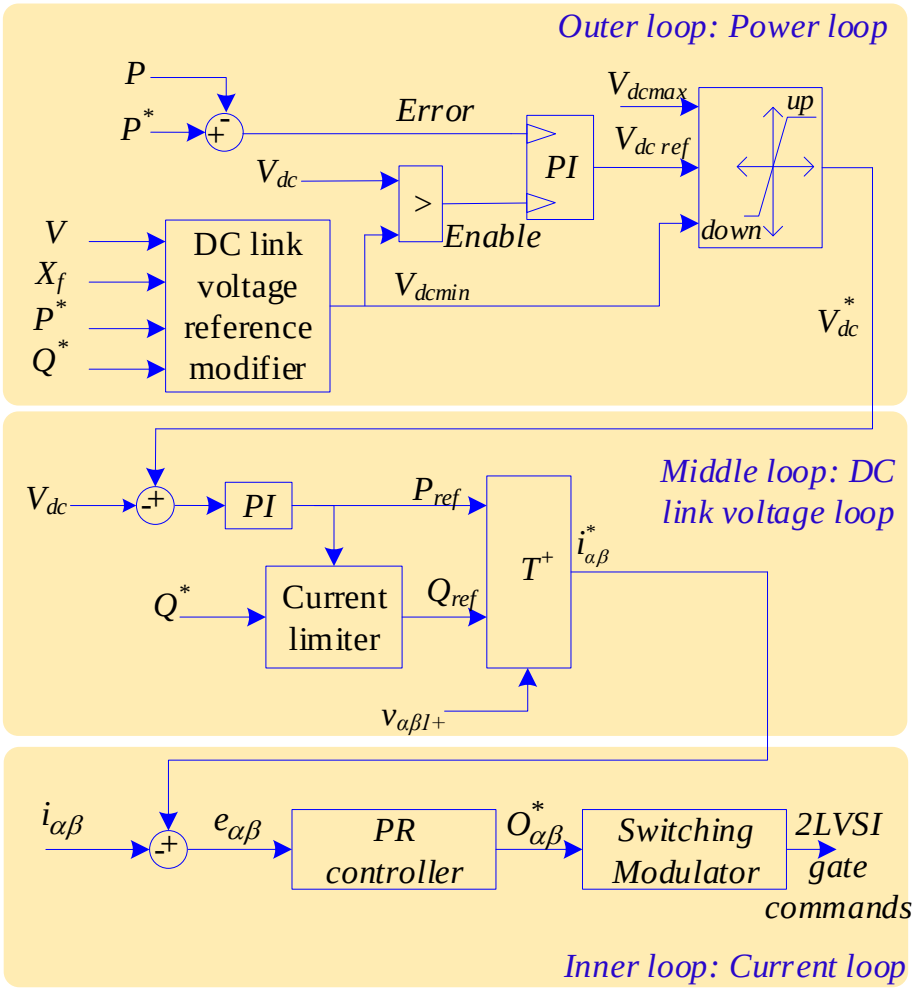

Figure 6. The proposed control scheme for the bioelectrochemical power-to-gas station.

3.1. DC Bus Voltage Reference Modifier

This part proposes a new DC bus voltage reference modifier to prevent converter instabilities. This method does not require the values of the grid voltage (V_g) or the equivalent grid impedance (Z_g), and certificates the converter to stay stable for any active and power references. Considering the equivalent circuit diagram of the system in Figure 7, the active and reactive powers (P and Q) absorbed by the 2L-VSC from the point of common coupling (PCC) can be written as follows:

$$P = \frac{V.V_i}{X_f} sin\delta = Ssin\delta, \tag{3}$$

$$Q = \frac{(VV_i cos\delta - V^2)}{X_f} = Scos\delta - \frac{V^2}{X_f} \tag{4}$$

where V, V_i and δ are PCC voltage, 2L-VSC voltage and angle, respectively. X_f is equal to $2 \times \pi \times f_o$ wherein f_o is the grid frequency in Hz, and S is apparent power. By squaring the relationships of P and Q in Equations (3) and (4) and arranging terms, the following expression can be obtained:

$$\left(Q + \frac{V^2}{X_f}\right)^2 + P^2 = S^2 sin^2\delta + S^2 cos^2\delta = S^2 \tag{5}$$

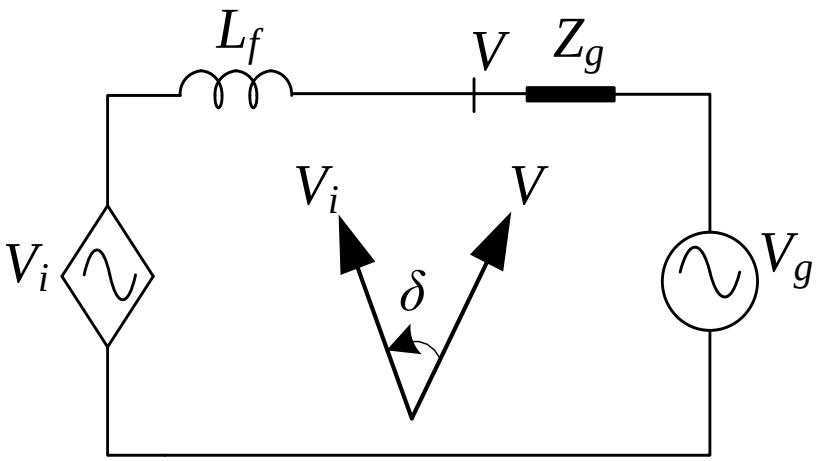

Figure 7. Modelling converter of the 2L-VSC as a voltage source.

Therefore, the converter must produce the following voltage to exchange power with the grid:

$$V_i = \frac{X_f}{V}\sqrt{\left(\left(Q + \frac{V^2}{X_f}\right)^2 + P^2\right)} \tag{6}$$

Therefore, the minimum DC bus voltage (V_{dcmin}) can be found as:

$$\begin{aligned} V_{dc\_min} &\geq \sqrt{3}V_i \\ \rightarrow V_{dc\min} &\geq \frac{X_f\sqrt{3}}{V}\sqrt{\left(\left(Q + \frac{V^2}{X_f}\right)^2 + P^2\right)} \end{aligned} \tag{7}$$

Figure 8 shows the minimum DC link voltage (V_{dcmin}) based on active and reactive powers. It can be concluded that V_{dcmin} is directly related to the reactive power and is almost independent of the active power.

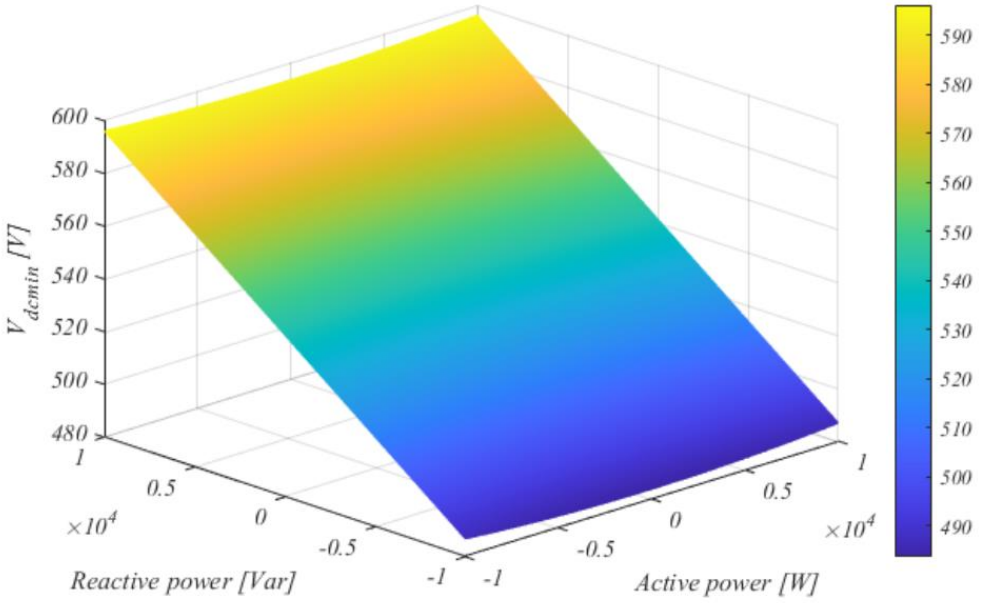

Figure 8. Minimum DC link voltage (V_{dcmin}) based on active and reactive powers.

3.2. Proposed PR Controller

The anti-windup of the PR controller and the DC voltage reference modifier must work complementary to each other. In the transient case, the anti-windup part of the PR controller limits the input of the switching modulator (SM) and avoids the saturation of the integral terms of the PR controller. In steady-state, the DC voltage reference modifier does not allow the reduction of the DC-link voltage lower than a specific value, avoiding the saturation of the controller. For drawing a sinusoidal current from the grid, a PR controller with harmonic compensation capabilities should be used. Typical ones can be expressed by Equation (8):

$$PR = K_p + \sum_{h=1,5,7,11,13} \frac{2K_{ih}\omega_{ch}s}{s^2 + 2\omega_{ch}s + h^2\omega_o^2} \tag{8}$$

where h, K_p, K_{ih}, ω_o and ω_{ch} are the harmonic order, the proportional coefficient, the resonant coefficients, the resonant frequency and the resonant bandwidths, respectively. The output of the PR controller (input of switching modulator) has to be smaller than the specific value O_{max}; otherwise, there will be over modulation. In over modulation, the switching frequency is reduced, and the waveforms at the converter's output are distorted.

The suggested anti-windup scheme for the PR controller consists of three main parts (see Figure 9): AC limiter, anti-windup for the resonant controller in fundamental frequency, and anti-windup for resonant controllers in the other frequencies. The AC limiter (ACL) to limit the input of SM can be considered as [32]:

$$O^*_{\alpha\beta} = \begin{cases} O_{\alpha\beta} & , \ |O_{\alpha\beta}| < O_{max} \\ \frac{O_{max}}{|O_{\alpha\beta}|} out_{\alpha\beta}, & |O_{\alpha\beta}| \geq O_{max} \end{cases} \\ where \ |O_{\alpha\beta}| = \sqrt{O_\alpha^2 + O_\beta^2} \tag{9}$$

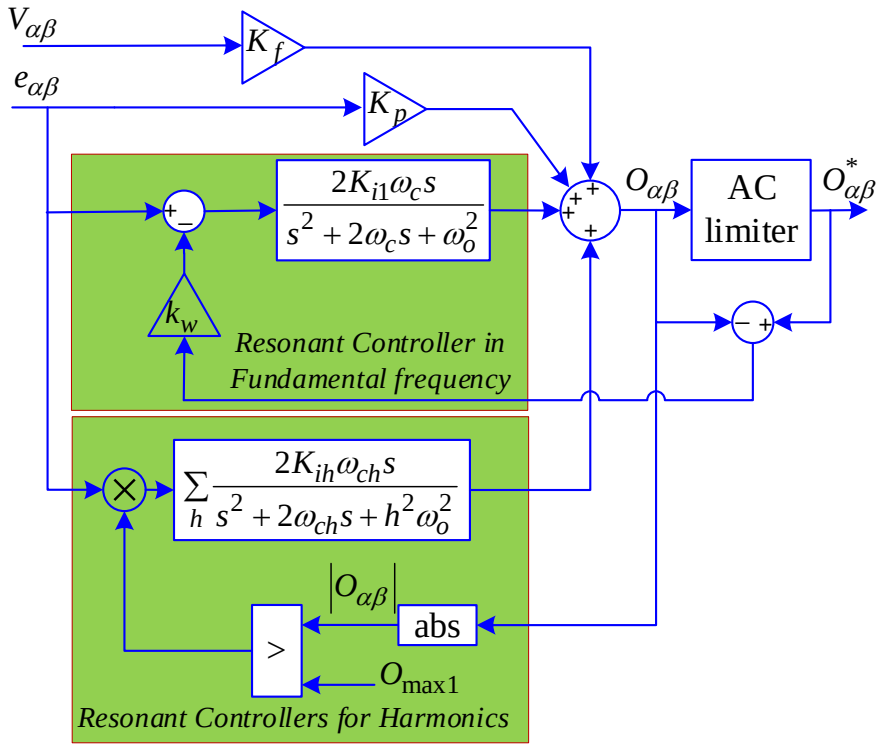

Figure 9. PR controller with the anti-wind-up capability and harmonic compensation capability in the inner current loop.

With this limiter, the SM input is not clipped and is always sinusoidal. The value of O_{max} is chosen based on the switching method.

The integrators within the controller may experience wind-up while a limiter hinders the output of a controller. In the proposed controller, the ACL is used inside of the anti-wind-up as the core block. If the absolute value of the output of the controller $|O_{\alpha\beta}|$ is more than the threshold O_{max1}, the harmonics compensation is cancelled, so that the controller still can track the current reference at the fundamental frequency. In addition, the difference between the AC limiter (ACL) and the controller's output lays mainly on the feedback signal to compensate the inputs of the integrators of the resonant controller in the fundamental frequency, so if the $|O_{\alpha\beta}|$ is going higher than threshold O_{max}, the output of the PR controller is clamped by the AC limiter and the input of the resonant controller in the fundamental frequency is modified by the anti-windup scheme.

The main essential variables in the anti-windup scheme are the maximum available outputs of the PR controller (O_{max} and O_{max1}), which should be chosen based on V_{dc}. The proposed values for thresholds are given as:

$$O_{max1} = V_{dc}\left(0.5 - \frac{t_{dead}}{T_s}\right), \tag{10}$$

$$O_{max} = V_{dc}\left(\frac{1}{\sqrt{3}} - \frac{t_{dead}}{T_s}\right), \tag{11}$$

where t_{dead} and T_s are the switching dead time and the switching period, respectively. The switching dead time reduces the maximum available output of the PR controller and also degrades the quality of the output current. However, these drawbacks can be easily overcome by using dead time compensation methods [33].

4. Processor-in-the-Loop Results

The Processor-in-the-Loop (PiL) studies were carried out by OPAL-RT OP4510 to verify the effectiveness of the proposed control system for a BES-P2G station. Figure 10 shows the schematic and setup of the implementation of the proposed system in OPAL-RT. The hardware part includes the EMG-BES model, switches, diodes, electrical components and voltage/current sensors as implemented in FPGA of OPAL-RT. The hardware part runs fast with a sample time of 875 ns. The control system is implemented in the CPU of OPAL-RT and runs slowly with a sample time of 10 µs. Due to the increase in the switching frequency, the time step of the real-time model should be much lower than the converter's switching time step. Typical CPU-based real-time simulation can only realize a minimum time step of Ts $\geq$ 10 µs, which is affected by the large bus latencies in a CPU. Also, the OP4510 connects to an oscilloscope to monitor voltage, current and electrical power in real-time. The values of currents and voltages are routed from the FPGA based model to the DAC channels.

The parameters of 2L-VSC in the proposed BES-P2G are listed in Table 2. A 10 kW EMG-BES module is modelled based on [10], where it is supposed that 10 stacks with 70 V and 14.25 A rating are installed in series. Two simulations have been done to verify the performance of the proposed control system.

In the first test, the active power reference stepped up from zero to its nominal value (10 kW) and the reactive power reference was set to 0 Var. The obtained results are illustrated in Figures 11 and 12. It can be seen in Figure 11 that, although the reference power is zero, the DC bus voltage is limited to 543 V to prevent system instability, and consequently, the active power absorbed by the 2L-VSC converter was non-zero. Once the reference of active power was changed from zero to 10 kW, the DC bus voltage increased, and the reference and instantaneous value of active power were precisely the same. As shown in Figure 11, the voltages of the LC filter's capacitors were constant, and the grid current increased with a convenient and fast transient response. According to Figure 12, the current reference in the stationary reference frame was correctly followed by the current

controller, and before increasing the power reference, the peak of the switching duty cycle was close to its maximum value, and the system was controlled at the boundary of stability and instability. By increasing the power reference and the DC bus voltage, the value of the switching duty cycle was reduced, and the converter worked in the linear region. This fact can be seen in Figure 12, where the peak of the switching duty cycle reduces from 1 to 0.85 after increasing the active power reference. The dynamics of the DC voltage variations are also shown in Figure 12, which had the same behavior as a first-order system with a rise time of 60 ms and there was no overshoot in DC voltage.

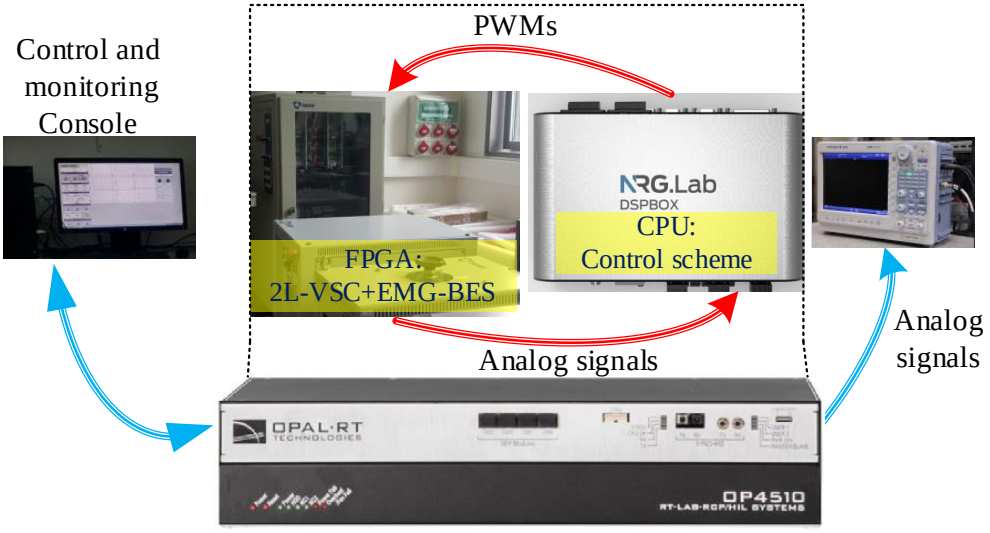

Figure 10. Processor-in-the-Loop (PiL) setup.

Table 2. 2L-VSC parameters.

Parameter	Value
Grid voltage	380 V–50 Hz
Grid short circuit capacity (SCC)	10 kA
Nominal power	10 kVA
LC filter inductor (Lf)	3.4 mH
LC filter capacitor (Cf)	5 µF
Switching frequency	10 kHz
Dead time	1 µs
DC link capacitor (C)	2200 µF

The results for reducing active power reference from 10 kW to zero are shown in Figures 13 and 14. The most important event happens at the moment that the active power reference changes: the DC voltage reference modifier and anti-windup of the P + R controllers prevent the switching duty cycle and system instability from increasing. The DC bus voltage decreases gradually in 40 ms, thus it is possible to continue connecting the proposed system to the grid.

The presented results show that BES-P2G with the proposed control can exchange power with the grid with a good transient response and zero steady-state error.

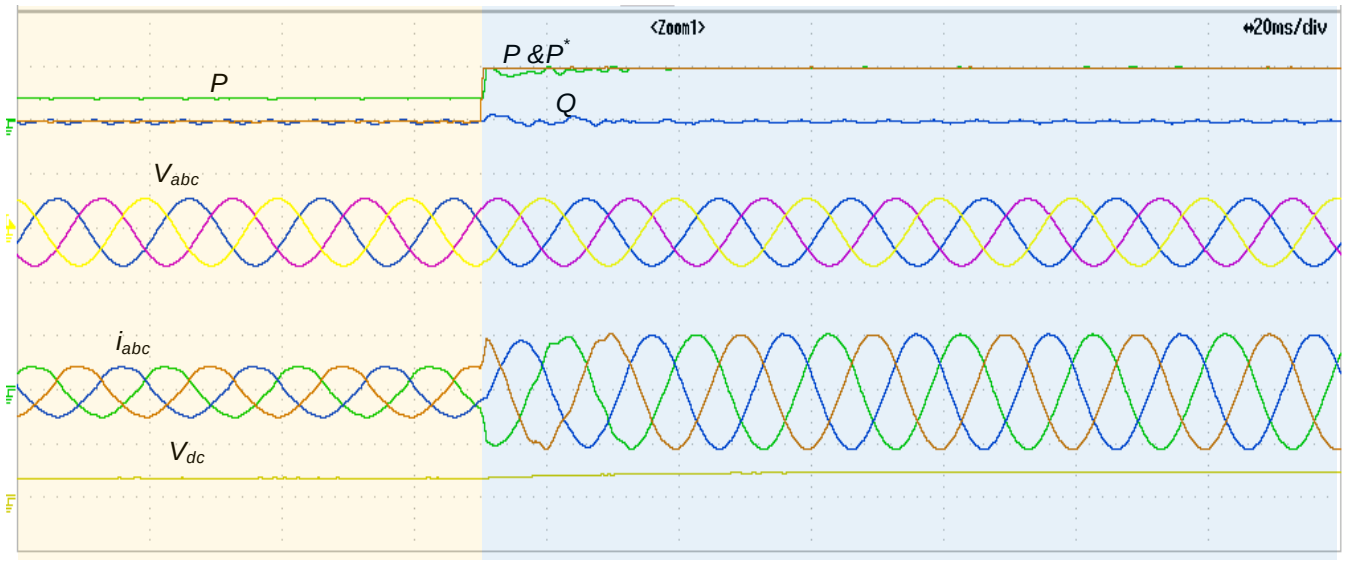

Figure 11. Real-time simulator results: active power reference step-up for BES-P2G. From top: active power reference (P*, 10 kW/div), active power (P, 10 kW/div), reactive power (Q, 10 kVAR/div), grid voltage (V_{abc}, 1000 V/div), grid current (i_{abc}, 20 A/div), DC link voltage (V_{dc}, 1400 V/div).

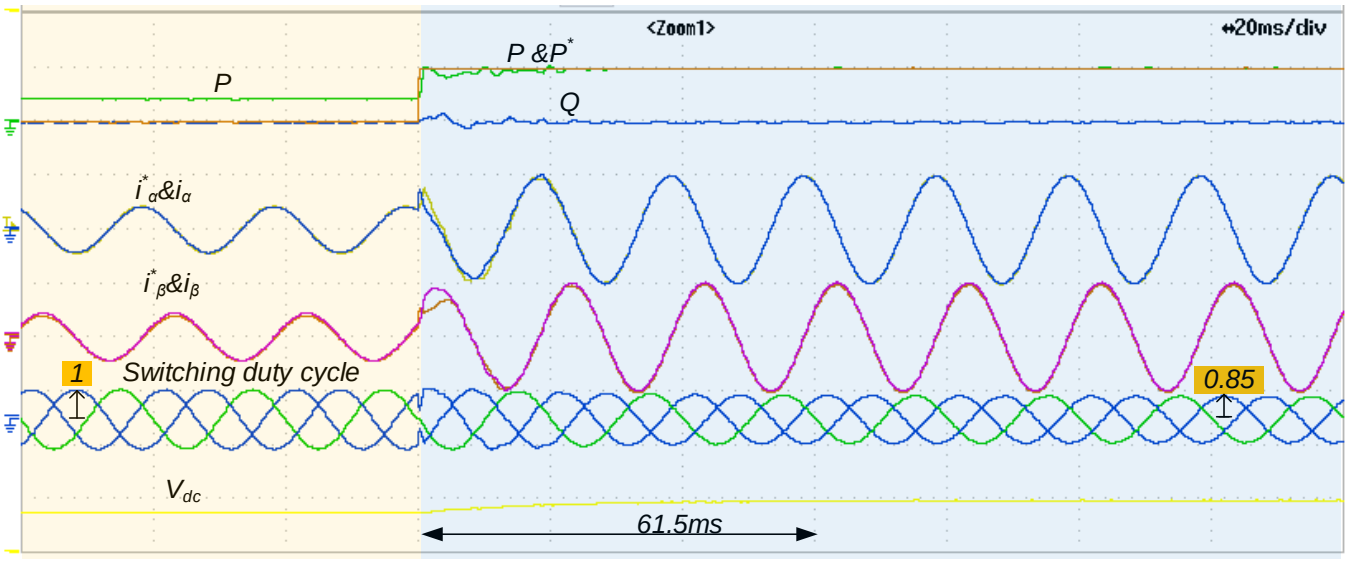

Figure 12. Real-time simulator results: active power reference step-up for BES-P2G. From top: active power reference (P*, 10 kW/div), active power (P, 10 kW/div), reactive power (Q, 10 kVAR/div), actual and reference currents ($i^*_{\alpha\beta}$&$i_{\alpha\beta}$), switching duty cycle, DC link voltage (V_{dc}, 700 V/div).

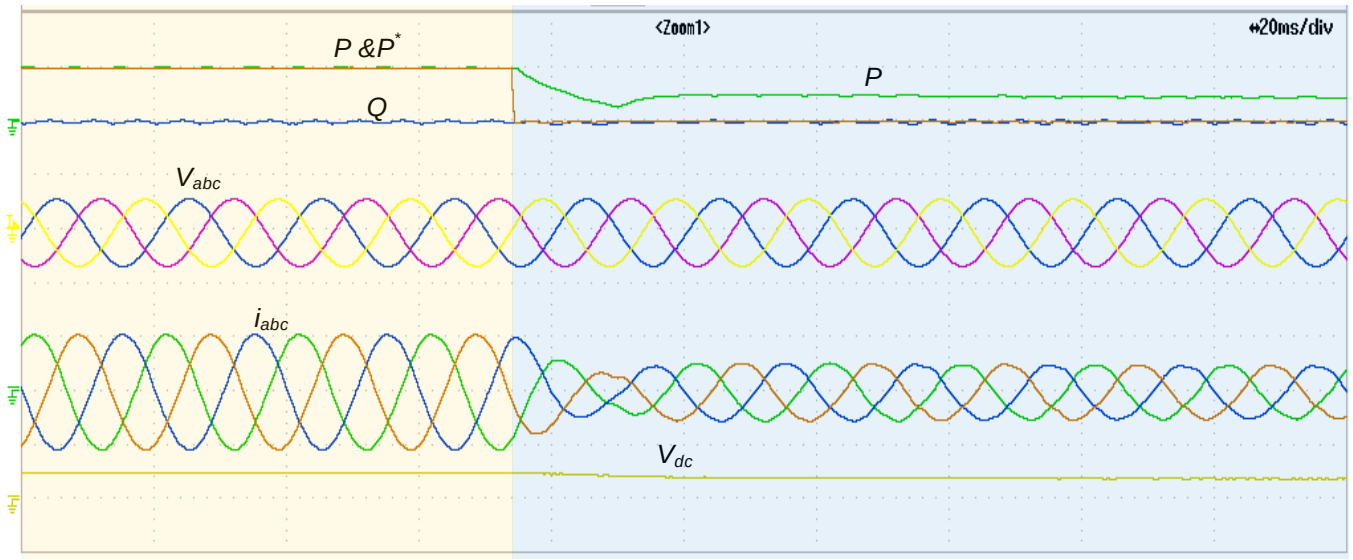

Figure 13. Real-time simulator results: active power reference step-down for BES-P2G. From top: active power reference (P*, 10 kW/div), active power (P, 10 kW/div), reactive power (Q, 10 kVAR/div), grid voltage (V_{abc}, 1000 V/div), grid current (i_{abc}, 20 A/div), DC link voltage (V_{dc}, 1400 V/div).

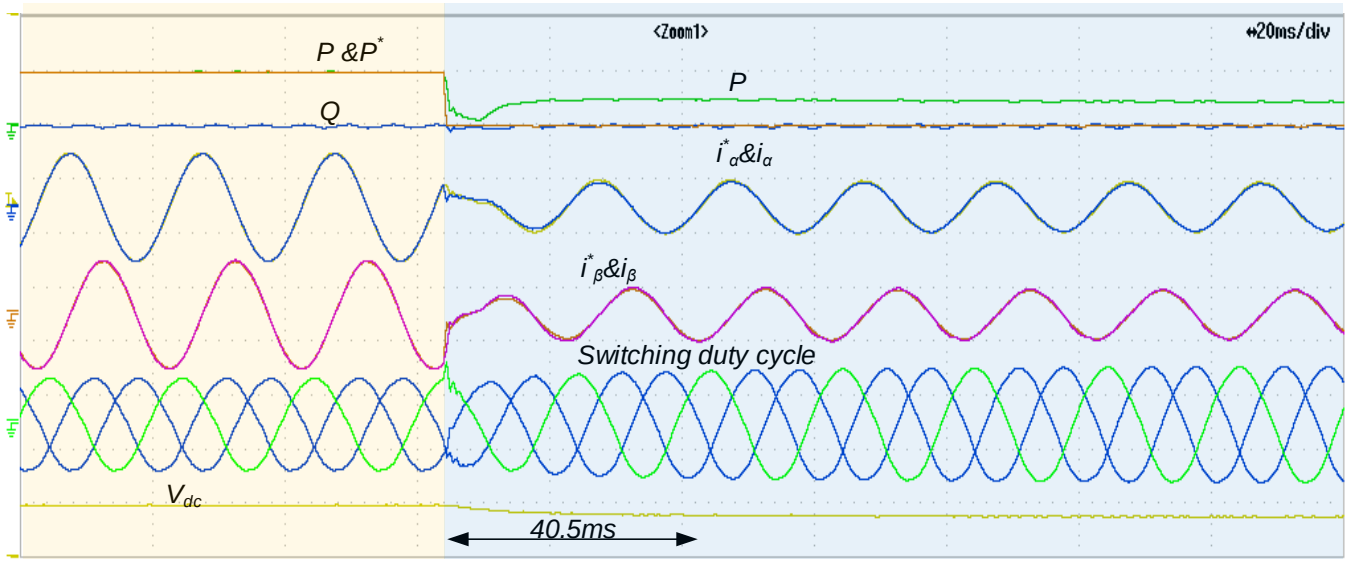

Figure 14. Real-time simulator results: active power reference step-down for BES-P2G. From top: active power reference (P*, 10 kW/div), active power (P, 10 kW/div), reactive power (Q, 10 kVAR/div), actual and reference currents ($i^*_{\alpha\beta}$&$i_{\alpha\beta}$), switching duty cycle, DC link voltage (V_{dc}, 700 V/div).

5. Conclusions

In this paper, an advanced control scheme has been designed and tested for a two-level voltage source converter-based BES-P2G plant. The data of a real medium-scale EMG-BES stack operating in different electrical conditions were considered to find a suitable and reliable equivalent-circuit model of the BES-P2G stack. Afterwards, a cascaded control scheme based on three loops, including power-voltage-current loops, was proposed to achieve goals as follows: (1) track power references, (2) avoid converter uncontrollability, and (3) keep the grid current sinusoidal. This paper proved that reducing the power reference of a BES-P2G plant may cause uncontrollability. Therefore, firstly, the power loop restricts the voltage reference value to keep the system stable. Secondly, the current

reference was clamped by the voltage loop to meet the converter current limitation. Thirdly, a new PR controller with anti-windup capability in fundamental frequency and harmonics was introduced as the current controller to keep the output currents always limited and sinusoidal. The results of the implementation of the proposed control system plant in OPAL-RT OP4510 set-up verified that the system is able to exchange power with the grid with a good performance.

Author Contributions: M.S. proposed the control scheme, conducted the analysis and validated the method. A.R. helped with control scheme development, and A.T. and J.D.V.L.R. were involved in capturing OPAL-RT results. A.L. and M.S. wrote and revised the paper. All authors have read and agreed to the published version of the manuscript.

Funding: This research was funded by the European Union's Horizon 2020 research and innovation program under the Marie Skłodowska-Curie, grant number 712949 and the Spanish Ministry of Economy and Competitiveness under the project RTI2018-100921-B-C21.

Acknowledgments: The research leading to these results has received funding from the European Union's Horizon 2020 research and innovation program under the Marie Skłodow-ska-Curie grant agreement No 712949 (TECNIOspring PLUS) and from the Agency for Business Competitiveness of the Government of Catalonia. This work has been also supported by the Spanish Ministry of Economy and Competitiveness under the project RTI2018-100921-B-C21.

Conflicts of Interest: The authors declare no conflict of interest.

References

1. Shahparasti, M.; Mohamadian, M.; Baboli, P.T.; Yazdianp, A. Toward power quality management in hybrid AC-DC microgrid using LTC-L utility interactive inverter: Load voltage-grid current tradeoff. *IEEE Trans. Smart Grid* **2017**, *8*, 857–867. [CrossRef]
2. Hirth, L. The market value of variable renewables: The effect of solar wind power variability on their relative price. *Energy Econ.* **2013**, *38*, 218–236. [CrossRef]
3. Shahparasti, M.; Mohamadian, M.; Parsa Moghaddam, M.; Teimourzadeh Baboli, P.; Haghifam, M.R. Energy management and operation modelling of hybrid AC–DC microgrid. *IET Gener. Transm. Distrib.* **2014**, *8*, 1700–1711. [CrossRef]
4. Heydari, R.; Dragicevic, T.; Blaabjerg, F. High-bandwidth secondary voltage and frequency control of VSC-Based AC microgrid. *IEEE Trans. Power Electron.* **2019**, *34*, 11320–11331. [CrossRef]
5. Schiebahn, S.; Grube, T.; Robinius, M.; Tietze, V.; Kumar, B.; Stolten, D. Power to gas: Technological overview, systems analysis and economic assessment for a case study in Germany. *Int. J. Hydrogen Energy* **2015**, *40*, 4285–4294. [CrossRef]
6. Shi, M.; Chen, X.; Zhou, J.; Chen, Y.; Wen, J.; He, H. Advanced secondary voltage recovery control for multiple hesss in a droop-controlled DC microgrids. *IEEE Trans. Smart Grid* **2018**, *10*, 3828–3839. [CrossRef]
7. Aryani, D.R.; Kim, J.S.; Song, H. Interlink converter with linear quadratic regulator based current control for hybrid AC/DC microgrid. *Energies* **2017**, *10*, 1799. [CrossRef]
8. Hajiaghasi, S.; Salemnia, A.; Hamzeh, M. Hybrid energy storage system for microgrids applications: A review. *J. Energy Storage* **2019**, *21*, 543–570. [CrossRef]
9. Ceballos-Escalera, A.; Molognoni, D.; Bosch-Jimenez, P.; Shahparasti, M.; Bouchakour, S.; Luna, A.; Guisasola, A.; Borràs, E.; Della Pirriera, M. Bioelectrochemical systems for energy storage: A scaled-up power-to-gas approach. *Appl. Energy* **2019**, *260*, 114138. [CrossRef]
10. Shahparasti, M.; Bouchakour, S.; Luna, A.; Molognoni, D.; Bosch-Jimenez, P.; Borràs, E. Simplified modelling of nonlinear electromethanogenesis stack for power-to-gas applications. *J. Energy Storage* **2020**, *31*, 101633. [CrossRef]
11. Eveloy, V.; Gebreegziabher, T. A Review of Projected Power-to-Gas Deployment Scenarios. *Energies* **2018**, *11*, 1824. [CrossRef]
12. Lewandowska-Bernat, A.; Desideri, U. Opportunities of power-to-gas technology in different energy systems architectures. *Appl. Energy* **2018**, *228*, 57–67. [CrossRef]
13. Götz, M.; Lefebvre, J.; Mörs, F.; McDaniel Koch, A.; Graf, F.; Bajohr, S.; Reimert, R.; Kolb, T. Renewable power-to-gas: A technological and economic review. *Renew. Energy* **2016**, *85*, 1371–1390. [CrossRef]
14. Götz, M.; Koch, A.M.; Graf, F. State of the art and perspectives of CO_2 methanation process concepts for power-to-gas applications. In Proceedings of the International Gas Union Research Conference, Copenhagen, Denmark, 17–19 September 2014.
15. Bailera, M.; Lisbona, P.; Romeo, L.M.; Espatolero, S. Power to Gas projects review: Lab, pilot and demo plants for storing renewable energy and CO_2. *Renew. Sustain. Energy Rev.* **2017**, *69*, 292–312. [CrossRef]
16. Cheng, S.; Xing, D.; Call, D.F.; Logan, B.E. Direct biological conversion of electrical current into methane by electromethanogenesis. *Environ. Sci. Technol.* **2009**, *43*, 3953–3958. [CrossRef] [PubMed]
17. Das, S.; Das, I.; Ghangrekar, M.M. Role of applied potential on microbial electrosynthesis of organic compounds through carbon dioxide sequestration. *J. Environ. Chem. Eng.* **2020**, *8*, 104028. [CrossRef]

18. Rodríguez-Alegre, R.; Ceballos-Escalera, A.; Molognoni, D.; Bosch-Jimenez, P.; Galí, D.; Licon, E.; Della Pirriera, M.; Garcia-Montaño, J.; Borràs, E.; Rodríguez-Alegre, R.; et al. Integration of membrane contactors and bioelectrochemical systems for CO_2 conversion to CH_4. *Energies* **2019**, *12*, 361. [CrossRef]
19. Zeng, Q.; Fang, J.; Li, J.; Chen, Z. Steady-state analysis of the integrated natural gas and electric power system with bi-directional energy conversion. *Appl. Energy* **2016**, *184*, 1483–1492. [CrossRef]
20. Power to Gas in a Decarbonized European Energy System based on Renewable Energy Sources; Infotech Report. Available online: https://www.storeandgo.info/fileadmin/dateien/STORE_GO_power_to_gas_roadmap_update.pdf (accessed on 18 June 2021).
21. Molognoni, D.; Bosch-Jimenez, P.; Rodríguez-Alegre, R.; Marí-Espinosa, A.; Licon, E.; Gallego, J.; Lladó, S.; Borràs, E.; Della Pirriera, M. How operational parameters affect electromethanogenesis in a bioelectrochemical power-to-gas prototype. *Front. Energy Res.* **2020**, *8*, 174. [CrossRef]
22. Friis Pedersen, C.; Raskmark Rønne, R. An Efficient AC-DC Electrical Power Converting Unit Configuration. European Patent Application No. EP2963761A1, 17 June 2015.
23. Muñoz-Aguilar, R.S.; Molognoni, D.; Bosch-Jimenez, P.; Borràs, E.; Della Pirriera, M.; Luna, Á. Design, operation, modeling and grid integration of power-to-gas bioelectrochemical systems. *Energies* **2018**, *11*, 1947. [CrossRef]
24. Shahparasti, M.; Rocabert, J.; Muñoz, R.S.; Luna, A.; Rodríguez, P.; Munoz, R.S.; Luna, A.; Rodriguez, P. Smart AC storage based on microbial electrosynthesis stack. In Proceedings of the 2018 7th International Conference on Renewable Energy Research and Applications (ICRERA), Paris, France, 14–17 October 2018; Volume 5, pp. 1086–1091. [CrossRef]
25. Zhang, Y.; Angelidaki, I. Microbial electrolysis cells turning to be versatile technology: Recent advances and future challenges. *Water Res.* **2014**, *56*, 11–25. [CrossRef]
26. Blasco-Gómez, R.; Batlle-Vilanova, P.; Villano, M.; Balaguer, M.D.; Colprim, J.; Puig, S. On the edge of research and technological application: A critical review of electromethanogenesis. *Int. J. Mol. Sci.* **2017**, *18*, 874. [CrossRef]
27. Soavi, F.; Santoro, C. Supercapacitive operational mode in microbial fuel cell. *Curr. Opin. Electrochem.* **2020**, *22*, 1–8. [CrossRef]
28. Do Park, J.; Roane, T.M.; Ren, Z.J.; Alaraj, M. Dynamic modeling of a microbial fuel cell considering anodic electron flow and electrical charge storage. *Appl. Energy* **2017**, *193*, 507–514. [CrossRef]
29. Liserre, M.; Blaabjerg, F.; Hansen, S. Design and control of an LCL-filter-based three-phase active rectifier. *IEEE Trans. Ind. Appl.* **2005**, *41*, 1281–1291. [CrossRef]
30. Shahparasti, M. Distributed generation inverter: New control strategies to supply local load with standard voltage under distorted grid voltage. *J. Energy Manag. Technol.* **2019**, *3*, 1–10. [CrossRef]
31. Mohan, N.; Undeland, T.M. *Power Electronics: Converters, Applications, and Design*; John Wiley & Sons: Hoboken, NJ, USA, 2007; ISBN 0471226939.
32. Shahparasti, M.; Catalán, P.; Roslan, N.F.; Rocabert, J.; Muñoz-Aguilar, R.-S.; Luna, A.; Shahparasti, M.; Catalán, P.; Roslan, N.F.; Rocabert, J.; et al. Enhanced control for improving the operation of grid-connected power converters under faulty and saturated conditions. *Energies* **2018**, *11*, 525. [CrossRef]
33. Buso, S.; Mattavelli, P. *Digital Control in Power Electronics*; Morgan & Claypool: San Rafael, CA, USA, 2006; Volume 2, ISBN 1598291130.